*J. Water Environ. Nanotechnol., 6(4): 338-355 Autumn 2021*

ORIGINAL RESEARCH PAPER

# Green Synthesis of Iron Nanoparticles Using Bioflocculant Extracted from Okra (*Abelmoschus esculentus* (L) Moench) and Its Application towards Elimination of Toxic Metals from Wastewater: A Statistical Approach

***Ashwini Prabhakar Shende, Nilanjana Das****

[1] *Bioremediation Laboratory, School of Bio Sciences and Technology, VIT, Vellore 632014, Tamil Nadu, India.*

Received: 2021-05-21 Accepted: 2021-07-23 Published: 2021-08-01

**ABSTRACT**

In recent years, the development in the field of nanotechnology is due to the fascinating properties of nanoparticles. In the present study, plant-based bioflocculant extracted from the fruits of Okra (*Abelmoschus esculentus*) was purified, characterized, and used for the biosynthesis of iron nanoparticles. Fourier transform infrared (FT-IR) spectral analysis revealed the presence of hydroxyl, carboxyl and sugar derivatives in the bioflocculant. The biosynthesized Fe nanoparticles were characterized using UV-vis spectroscopy, X-ray diffraction (XRD), Fourier transform infrared (FT-IR), Scanning electron microscopy (SEM), and Atomic force microscopy (AFM). TEM analysis was performed and the size of synthesized Fe nanoparticles was found to be 50 nm which was assessed by dynamic light scattering (DLS) analysis. Flocculation activity of bioflocculant mediated Fe nanoparticles (BFFeNPs) was tested. The effects of various parameters on Pb(II)removal using BFFeNPs were evaluated using response surface methodology (RSM) based on Box Behnken Design (BBD).The BFFeNPs exhibited high Pb (II) removal efficiency (91.45%) under optimized parameters viz. pH 6, BFFeNPs dosage 0.2 g/L, contact time 30 min and temperature 30º C. A quadratic polynomial model was fit with the actual data of $R^2$ 0.99 for metal removal. To the best of our knowledge, this is the first report on the potential use of Okra bioflocculant mediated Fe nanoparticles synthesis for the cost-effective and eco-friendly removal of lead from wastewater.

**Keywords:** *Bioflocculant mediated Fe nanoparticles; Box Behnken Design (BBD); Flocculation activity; Heavy metal removal; Response surface methodology.*

**How to cite this article**

*Prabhakar Shende A., Das N. Green Synthesis of Iron Nanoparticles Using Bioflocculant Extracted from Okra (Abelmoschus esculentus (L) Moench) and Its Application towards Elimination of Toxic Metals from Wastewater: A Statistical Approach. J. Water Environ. Nanotechnol., 2021; 6(4): 338-355.*

*DOI: 10.22090/jwent.2021.04.005*

## INTRODUCTION

Tremendous development in the field of green nanotechnology has been noted due to environmental benefits, less time duration, and cost-effectiveness. Biosynthesis of nanoparticles is applied to different scientific disciplines including material science and biomedical applications [1]. Different methods viz. physical, chemical, and hybrid methods are being used for the synthesis of nanoparticles. The high toxicity of chemicals employed in these conventional methods limits their applications. Moreover, these methods generate toxic wastes which are hazardous to the environment and harmful to humans. Therefore, eco-friendly and green approaches are now being used as a replacement for those expensive, outdated and inefficient methods. Comparing the cost-effectiveness and side effects of the conventional methods, researchers are mainly focusing on biological approaches [2]. The nanoparticles generated by the biological process show higher catalytic activity improved contact between metal salt and enzyme, greater surface area to volume

* Corresponding Author Email: *nilanjanamitra@vit.ac.in*

ratio [3]. Nanoparticles exhibit their remarkable potential in the field of biology and medicine based on specific characteristics such as size, morphology, etc. [4].

Green synthesis of various nanoparticles using plant extract has been reported by several workers. Sayadi et al. [5] reported the green biosynthesis of palladium nanoparticles using *Spirulina platensis* algal extract. In addition, Yazdani et al. [6] also reported the green synthesis of palladium oxide nanoparticles using *Dictyota indica* seaweed for adsorption.

Heavy metal pollution is becoming one of the most serious environmental problems globally [7]. The treatment of wastewater containing heavy metals is mandatory due to their persistence in the environment. In order to detoxify heavy metals, different techniques like photocatalytic oxidation, UV irradiation, electrochemical, bioremediation, ion-exchange, chemical coagulants, ozonation, reverse osmosis, and adsorption have been employed [8]. Among these technologies, the use of nano-based adsorbents is the more convenient method for the removal of heavy metals from the aqueous environment [9]. The application of iron oxide-based nanomaterial is more attractive for heavy metal removal from contaminated wastewater due to their important features like small size, high surface area, and magnetic properties [10]. Arsenic removal from mining effluent was reported using plant-mediated green synthesized iron nanoparticles [11]. Efficient removal of lead from aqueous solution using $FeNi_3$@$SiO_2$ magnetic nanocomposite was reported [12]. Removal of nickel and chromium from aqueous solution using Copper oxide nanoparticles was reported by Hosseini et al. [13].

Among the toxic metals, lead (Pb) is in the limelight due to its major impact on the environment. Chronic exposure to high amounts of Pb (II) can result in various and extensive damages to systems of the body, reproductive system, basic cellular processes, and brain functions. Furthermore, lead poisoning causes high blood pressure, anemia, insomnia, liver disease, bone cancer, headache, dizziness, irritability, weakness of muscles, hallucination and renal damage, coma and ultimately causing death [14]. Therefore, the removal of Pb (II) from the wastewater is mandatory.

Bioflocculants have gained tremendous attention owing to their unique flocculating characteristics, harmlessness, non-toxic and biodegradable nature which aids in creating an eco-friendly environment [15]. They serve as a replacement for chemical-based flocculants [16] and are widely used in various fields including synthesis of nanoparticles, removal of heavy metal and dyes, mineral processing, drinking water, and wastewater treatment, etc. [17, 18].

There are reports on the use of microbial bioflocculants for the removal of heavy metals from an aqueous environment [19]. Application of bioflocculant passivated copper nanoparticles on wastewater treatment has been reported recently [17]. But reports are scanty on bioflocculant mediated nanoparticles for the removal of heavy metals from an aqueous environment.

Fe nanoparticles have attracted much attention due to their unique properties including superparamagnetism, surface volume ratio, greater surface area, and easy separation methodology. Fe nanoparticles have a great potential for their applications as wastewater treatment adsorbents, catalytic materials, pigments, gas sensors, coatings, ion exchangers, magnetic data storage devices, magnetic recording devices, magnetic resonance imaging, and bio-separation [20]. It is well-established fact that iron nanoparticles show greater catalytic activities for dye reduction and removal. There has been a great interest in using plant extract in synthesizing the Fe nanoparticles for industrial applications. The iron nanoparticles are safer and cheaper [21].

Therefore, the current study is focused on the green synthesis of iron nanoparticles (FeNPS) using bioflocculant extracted from Okra and its application towards the removal of Pb (II) from wastewater. The statistical optimization of the metal removal process was done using response surface methodology (RSM).

## MATERIALS AND METHODS

### *Chemicals*

All chemicals viz. ferric nitrate ($Fe(NO_3)_3$, ethanol, methanol, acetone, glucose, bovine serum albumin, and trifluoroacetic acid were purchased from Himedia company and used without further purification.

### *Plant Material*

The plant Okra (*Abelmoschus esculentus* (L) Moench) belonging to the family Malvaceae is widely grown through tropical and subtropical

regions of the country. Fruits were purchased from the local vegetable market located at Vellore, Tamil Nadu, India, and used for the study.

*Collection and analysis of wastewater*

The wastewater sample was collected from a Common Effluent Treatment Plant (CETP) located in Ranipet, Vellore, Tamil Nadu, India. The Physico-chemical characteristics of the wastewater sample were analyzed using standard analytical methods [22]. The presence of heavy metals viz. $Ni^{2+}$, $Zn^{2+}$, $Cd^{2+}$, $Cu^{2+}$ and $Pb^{2+}$ was determined using Atomic Absorption Spectrophotometer (AAS) (VARIAN SPECTRA 240 model).

*Extraction and Purification of Okra Bioflocculant*

The fresh fruits of okra were sliced, homogenized, and extracted with cold water containing 1 % w/v of metabisulphite. The crude mucilage was centrifuged at 3000 rpm for 5 minutes, precipitated from the supernatant with acetone, and washed several times. The cream-colored product was obtained and dried under a vacuum in a desiccator. A light brown colored powder was obtained after the removal of complete moisture. The dried powder was pulverized and stored in a bottle at 4°C till used [23].

The dried powder of bioflocculant (BF) was poured into two volumes of ice-cold solvents such as ethanol, methanol, and acetone (1:2 v/v) to precipitate the bioflocculant. It was allowed to stand overnight at 4°C in the refrigerator. The resulting precipitate was separated by centrifugation at 10,000 rpm for 15 min and washed by redissolving in the double-distilled water followed by reprecipitation. The process was repeated twice. The precipitated bioflocculant was dehydrated for 2 hours for the removal of water and solvent in a vacuum using a rotary evaporator. The extract was subjected to dialysis against distilled water and kept overnight at 4°C [18].

*Characterization of Bioflocculant*

The purified bioflocculant was subjected to chemical characterization. The total carbohydrate content of bioflocculant was determined by the phenol-sulphuric acid method using glucose as a standard solution [24]. The total protein content of bioflocculant was determined using the Bradford method with bovine serum albumin as a standard [25]. The amino acid was estimated by the ninhydrin method [26]. After hydrolysis of the okra bioflocculant with 2 M, trifluoroacetic acid at 120°C for 2 h, neutral sugars, uronic acids, and amino sugars were determined with anthrone method, carbazole sulfate acid method, and the Elson-Morgan method, respectively [27]. Instrumental analysis viz. Fourier Transform Infra-red Spectroscopy (FT-IR), X-ray Diffraction (XRD), Scanning Electron Microscopy (SEM), Energy-dispersive X-ray spectroscopy (EDX), and Atomic Force Microscopy (AFM) analysis were also performed for characterization of purified bioflocculant.

*FTIR and XRD analysis*

The functional groups of purified bioflocculant were investigated using Fourier transform infrared (FTIR, PerkinElmer MA, USA). The dried sample was blended with KBr powder and pressed into pellets for FTIR spectra measurement spectrum in the frequency range of 500-4000 $cm^{-1}$ [18].

X-ray diffraction (XRD) patterns of bioflocculant were conducted with X' Pert Pro P analytical diffractometer, Germany using monochromatic Cu Kα X-ray radiation ($\lambda = 0.154$ nm) running at 40 kV and 30 mA [28].

*SEM, EDX, and AFM analysis*

Scanning electron microscopic studies were carried out to elucidate the surface morphology of the okra bioflocculant using HITACHI model (Carl Zeiss) high-resolution electron microscope to verify morphology and homogeneity of particles. Bioflocculant suspension was centrifuged at 10,000 rpm for 15 min. The pellets were resuspended in deionized double distilled water. A drop of the bioflocculant suspension was placed on a glass coverslip and air-dried. These samples were chemically fixed for 24 hours at 40°C using a final concentration of 2.5% glutaraldehyde. The sample was rinsed with distilled water 3 times to remove traces of glutaraldehyde. Then samples were dehydrated in grade series of ethanol (30, 50, 75, 85, 95, and 100%), and air-dried under vacuum [18].

The EDX analysis was done with an X-ray detector to examine the elemental constituent of the okra bioflocculant.

The surface topography of the bioflocculant was analyzed using Atomic force microscopy (AFM). About 5-10 mL of bioflocculant suspension was distributed on a mica disc (Pelco mica disc 10 mm) by a spin rotating plate and absolute ethanol was

dropped over the sample to fix it on the mica disc. Then, the mica sheet was air-dried to eliminate the residual ethanol [29]. The AFM images were captured by Nanosurf Easyscan 2, Switzerland.

*Bioflocculant mediated green synthesis and characterization of iron (Fe) nanoparticles*

The iron nanoparticles were synthesized using purified Okra bioflocculant. The Okra fruits (5 g) were washed thoroughly with distilled water and cut into fine pieces and were subsequently macerated in a 50 mL mixture of double distilled water and methanol (1:1). This liquefied mixture was subjected to centrifugation at 10,000 rpm for 5 min at 4°C and the supernatant was separated. The supernatant obtained was used as a reducing agent for the synthesis of the iron nanoparticles. For the synthesis of Fe nanoparticles, bioflocculant (5 ml) was added dropwise into the solution of 10 mM ferric nitrate ($Fe(NO_3)_3$ under magnetic stirring conditions. Later the content was placed onto a rotary orbital shaker at 200 rpm for 72 h at 30°C temperature under dark conditions. The reduction of Fe ions was monitored at intervals of 24 h followed by measurement of the UV–Vis spectra using a spectrophotometer (JASCO V-670 PC). To find out the maximum absorption, a spectral scanning analysis was carried out by measuring the optical density of the sample after 72 h using a UV–Vis spectrophotometer from wavelength 300-700 nm. The synthesized Fe nanoparticles were extracted by centrifuging the sample at 13,000 rpm for 10 min after 72 h of the incubation period. For removing the organic impurities, the recovered pellets were then washed with 50 ml of 1:1, methanol-water solution, and pellets were freeze-dried using a lyophilizer. The dried pellet of synthesized nanoparticles was ground into powder form and subjected to X-ray diffraction (XRD), Fourier-transform infrared spectroscopy (FTIR) [30], scanning electron microscopy (SEM) analysis, Energy-dispersive X-ray spectrometer (EDX) analysis [31], Atomic Force Microscopy (AFM) analysis following the standard method as demonstrated by Vitta et al. [32], Transmission electron microscopy (TEM) under an accelerating voltage of 100 kV (TECNAI G20 TWIN), and dynamic light scattering (DLS) (ZEN 3600, Malvern, Worcestershire, UK) [11].

*Flocculation assay using simulated wastewater containing heavy metals*

The heavy metal removal efficiency of the bioflocculant and bioflocculant mediated iron nanoparticles (BFFeNPs) was determined using simulated wastewater containing heavy metals. For this purpose, aqueous solutions containing $Ni^{2+}$, $Zn^{2+}$, $Pb^{2+}$, $Cd^{2+}$, and $Cu^{2+}$ at concentrations of 500 µg/L each were prepared. The biofocculation experiment was performed with purified bioflocculant and BFFeNPs. The samples were maintained at pH 7 and the final volume was made up to 50 mL. After the bioflocculant and BFFeNPs (0.2 g/L) were added, the samples were shaken on a rotary shaker at 150 rpm at 25° C, for 24 hours. After 24 hours the supernatant was filtered through a 0.45 µm syringe filter. The metal concentrations in the solution were measured with an Atomic Absorption Spectrometer (VARIAN SPECTRAA 240) as well [33].

The flocculating activity was calculated using the following equation :

$$\text{Flocculation activity (\%)} = \frac{F2 - F1}{F2} \times 100$$

Where F2 is the initial metal concentration and F1 is the final metal concentration.

*Heavy metal removal from real wastewater using BFFeNPs*

The experiment was conducted with a real wastewater sample collected from the Common Effluent Treatment Plant (CETP) and the procedure was followed as described above in the flocculation assay using simulated wastewater. Presence of heavy metals viz. $Ni^{2+}$, $Zn^{2+}$, $Cd^{2+}$, $Cu^{2+}$, and $Pb^{2+}$ were detected in the wastewater sample. Additionally, the effect of different parameters on Pb (II) removal from wastewater is studied.

*Effect of parameters on Pb (II) removal from real wastewater*

The effects of different parameters on Pb (II) removal from real wastewater was tested using different pH value (2-10), BFFeNPs dosage (0.1-0.5 gm/L), contact time (10-50 min), and temperature (25-50°C ) keeping the other parameters at optimal conditions [34].

*Process optimization for maximum Pb (II)removal*

Response surface methodology using Box-Behnken design was used to optimize various parameters viz. pH, BFFeNPs dosage, contact time, and temperature for the maximum removal of Pb (II) metal ion. The quadratic model was used to analyze the data. Each factor in the design was

Table 1. Independent factors and its level used in response surface design for Pb (II) removal (%)

| Factors | Name | Low level (-1) | Level ($0^{th}$) | High level (+1) |
|---|---|---|---|---|
| A | pH | 2 | 6 | 10 |
| B | BFFeNPs dosage (g/L) | 0.1 | 0.2 | 0.3 |
| C | Contact time (min) | 10 | 30 | 50 |
| D | Temperature (°C) | 10 | 30 | 50 |

studied at 3 different levels (−1, 0, +1) and the minimum and maximum ranges of pH, BFFeNPs dosage, contact time, and temperature variables were determined as shown in Table 1.

A design of 29 experiments was formulated and experiments were carried out in 250 mL Erlenmeyer flasks containing wastewater (100 mL) with different pH, BFFeNPs dosage, contact time, and temperature. Pb (II) removal percentages were evaluated as response 1. The 3D contour plots were prepared to evaluate the interaction between the optimized parameters, which influence the responses. The respective responses were analyzed by using a second-order polynomial equation, and the data were fitted to the equation by multiple regression procedures.

Later, an experiment was conducted in triplicates using the optimum values for variables viz. pH, BFFeN dosage, contact time, and temperature given by response surface optimization to validate the predicted value and the experimental value of the responses. The results of the experimental design were analyzed and interpreted using Design-Expert version 12.0 (Minneapolis, MN, USA) statistical software.

## RESULTS AND DISCUSSION

*Analysis of wastewater*

The wastewater sample collected from a Common Effluent Treatment Plant (CETP) located in Ranipet, was black, giving a pungent smell with a temperature (28°C). The pH of wastewater was slightly alkaline (7.5). TDS and TSS in the wastewater sample were 5,534 mg/L and 2563 mg/L respectively. High values of COD were observed (1200 mg/L) compared to BOD (580.30 mg/L). Sulfate and nitrate were found to be 326 mg/L and 4.4 mg/L respectively. The average amount of heavy metal ions $Cu^{2+}$, $Cd^{2+}$, and $Pb^{2+}$ were higher whereas $Ni^{2+}$ and $Zn^{2+}$ concentrations were observed as < 2 mg/L.

*Characterization of okra bioflocculant*

The chemical composition of bioflocculants plays an important role in their flocculating activities. Bioflocculants contain proteins, glycoproteins, polysaccharides, lipids, and glycolipids [35].

In this study, a chemical analysis of the purified okra bioflocculant revealed that it was a sugar-protein derivative composed of carbohydrate (9.69%) and protein (19%) including neutral sugar, uronic acid, and amino sugar. Similar results were reported by Assi et al. and Acikgoz et al. where the total carbohydrate and protein content from Okra bioflocculant was found to be 9.75±7.69% and 19% respectively [36, 37].

*FTIR and XRD analysis*

The major functional groups present in okra bioflocculant were identified by Fourier transform infrared spectroscopy. The FTIR spectrum of bioflocculant extracted from okra was shown in Fig.1(a)which exhibited different peaks at different positions. The peak in the region of 1026.87 $cm^{-1}$ refers to the stretching of the C-O-C group in polysaccharides. The band at 3279.34 $cm^{-1}$is characteristics of stretching and deformations of the hydroxyl groups (OH). The absorption bands around 1200–800 $cm^{-1}$ are considered characteristic polysaccharide bands. They indicate the presence of -C-O- bonding of alcohol and ether. Similar results were demonstrated by Freitas et al. [38]. The sharp peaks at 2923.25 $cm^{-1}$and 2851.06 $cm^{-1}$ were corresponding to the asymmetric and symmetric stretching of the group -CH-$CH_2$ exists in fatty acids, a similar result was described by Swelam [39]. A significant band in the spectrum was observed between 1719 $cm^{-1}$ to 1233 $cm^{-1}$ resembling the presence of the carboxylic group. The absorption band at 1719 $cm^{-1}$ attributed to the C=O stretching mode of either methylated or protonated (non-ionized) form of a carboxyl group. The band at 1412.57 $cm^{-1}$ indicated the presence of C-H symmetrical deformation vibration. These functional groups serve as active sites for the attachment of colloidal particles and bioflocculant [38].

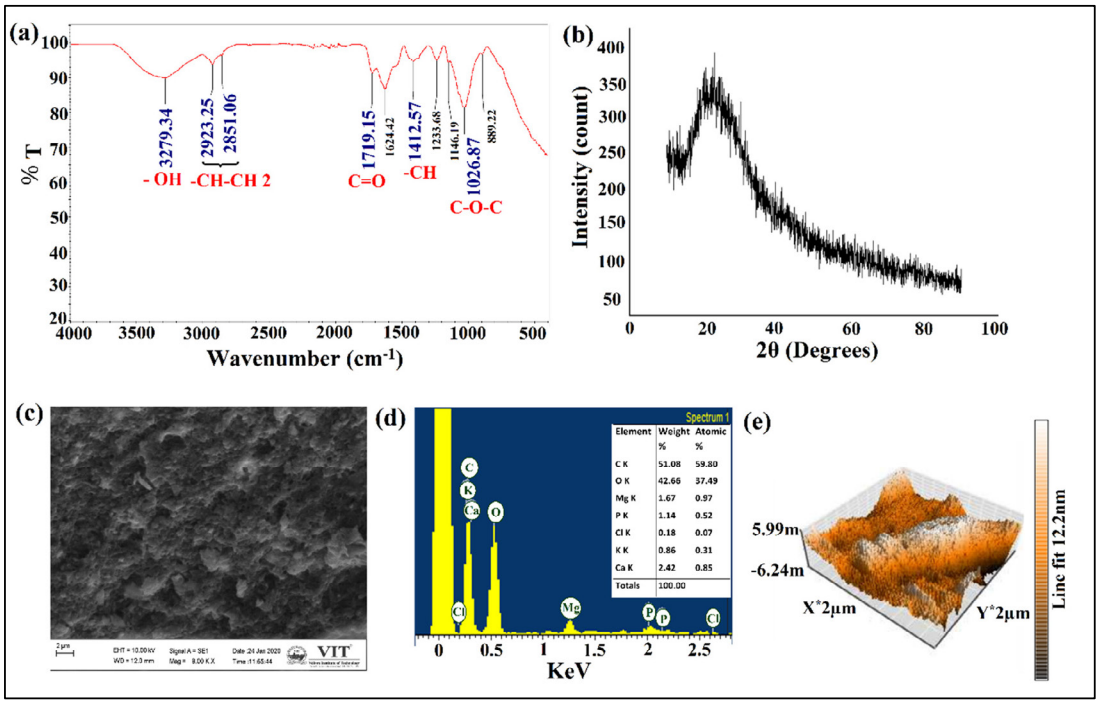


Fig. 1. Characterization of purified Okra bioflocculant using (a) Fourier-transform infrared spectroscopy (FTIR), (b) X-ray diffraction (XRD) analysis, (c) Scanning electron Microscopy (SEM), (d) Energy-dispersive X-ray spectroscopy (EDAX), and (e) Atomic force microscopy (AFM) analysis.

Fig. 1(b) shows the X-ray diffractogram of okra bioflocculant shows a broad peak and several halos with weak peaks and abundant noise in the band of $10^{\circ} < 2\theta < 80^{\circ}$, which gives the characteristic patterns of an almost completely amorphous nature where the disordered state of molecules produces scattered bands. A similar XRD pattern was illustrated by Freitas et al. [38].

*SEM, EDAX, and AFM analysis*

The SEM images of the okra bioflocculant, were studied to examine its morphology and microstructure as shown in Fig. 1(c). The surface micrograph of okra bioflocculant revealed irregular and amorphous structures.

The EDX spectrum of okra bioflocculant was shown in Fig. 1(d), which indicated the presence of carbonaceous material with a carbon weight percentage of 51.08% and oxygen weight percentage of 42.66%. The presence of C revealed that the okra bioflocculant contained proteins which contributed to the efficiency of the material in the process of heavy metal removal [32]. Fig. 1(d) inset) shows the weight percentage of the inorganic element Mg, P, Cl, K and Ca which was detected from okra bioflocculant. Similar results were illustrated by Emeje et al. [40].

AFM is a high-resolution tool which was widely used in polysaccharide surface morphology characterization. As shown in Fig. 1(e), the 3D image of the okra bioflocculant displayed an irregular entanglement structure. These entangled appearances may be due to the Van der Waals force of attraction, intra and inter-molecular hydrogen bonds in acidic biopolymers [41].

*Characterization of bioflocculant mediated FeNPs (BFFeNPs)*

The instant change in color from yellow to black was observed after the mixing of ferric nitrate ($Fe(NO_3)_3$ with the Okra bioflocculant extracts at the ratio of 1:1. Fig. 2(a) inset), indicating the formation of FeNPs. UV spectrum shows the maximum absorption at three different wavelengths of 230 nm, 279 nm, and 305 nm which indicated the gradual formation of Fe nanoparticles as shown in Fig. 2(a). Huang et al. reported tea extract mediated synthesis of iron nanoparticles showed absorption maximum at 205 and 275 nm while Dhuper et al. demonstrated zero-valent Fe nanoparticles from leaf extract of *Magnifera indica* exhibited maximum absorption at 216-268 nm. Similar results on the

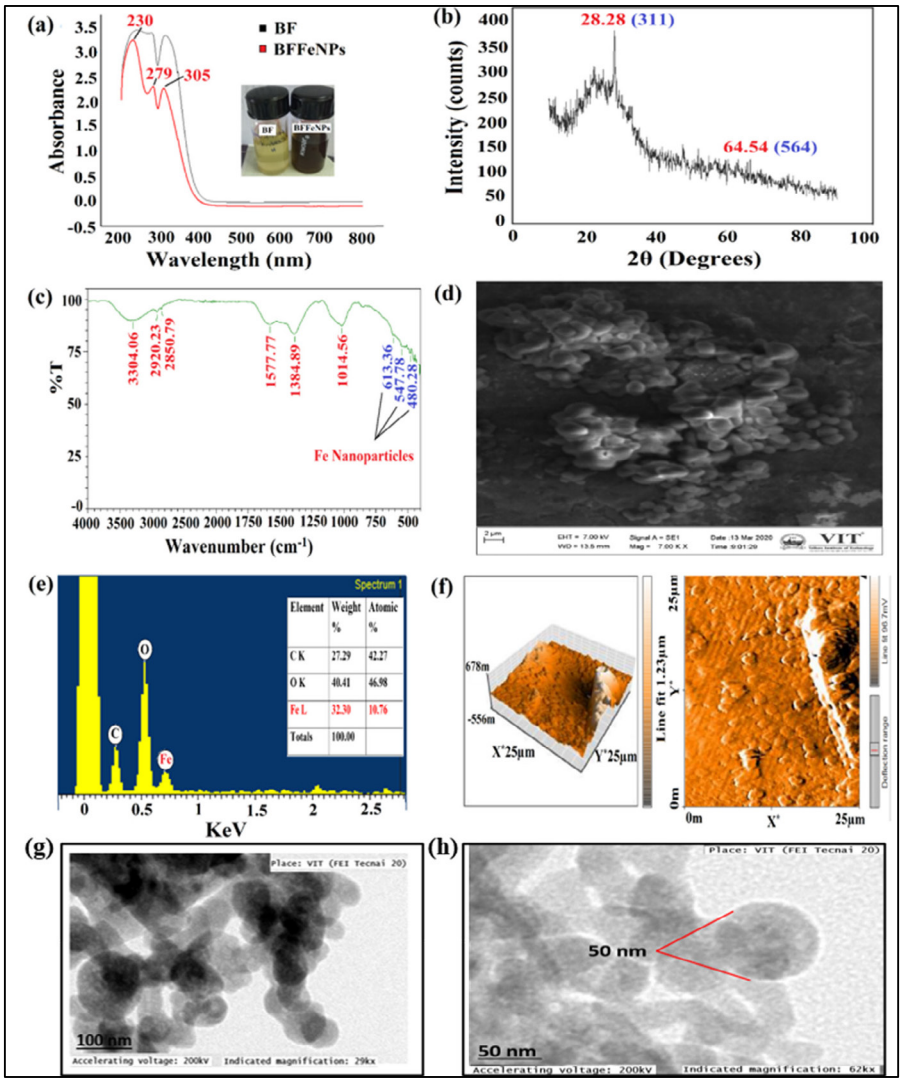


Fig. 2. Characterization of bioflocculant mediated iron nanoparticles ( BFFeNPs). (a) UV–visible spectrophotometry analysis of pure okra bioflocculant (BF) and synthesized Fe nanoparticles (BFFeNPs), (b) XRD analysis of synthesized Fe nanoparticles, (c) FTIR analysis of synthesized Fe nanoparticle, (d) SEM images of the synthesized Fe nanoparticles, (e) EDAX analysis of synthesized Fe nanoparticles and (f) AFM image of synthesized Fe nanoparticles, (g) and (h) TEM micrograph of synthesized nanoparticles.

biosynthesis of Fe nanoparticles using leaf extract were reported by Devatha et al. [42, 43, 44].

The XRD pattern of Fe nanoparticles exhibited well-defined peaks at 2θ values of 28.28 and 64.54 which correspond to the 311 and 564 and planes, respectively. As shown in Fig. 2(b), the intensity of Fe nanoparticles peaks at 2θ values of 28.28 and 64.54 reflected the high degree of crystallinity in Fe nanoparticles which were in good agreement with the results reported by Prasad et al. [30].

The FTIR spectrum of BFFeNPs is shown in Fig. 2(c). The peaks at 3304.06 $cm^{-1}$ are due to the O–H stretching vibration of free hydroxyl groups of alcohol. The twin peaks at 2920.23 and 2850.79 $cm^{-1}$ corresponded to the C-H tensile bond of alkanes [45, 46]. The absorption peaks at 1577.77 $cm^{-1}$, 1384.89 $cm^{-1,}$ and 1014.56 $cm^{-1}$ were attributed to C=C stretching vibration, C-H symmetric vibration, and C-H vibration respectively, which were characteristics functional group of bioflocculant. The small peak at 613.36 $cm^{-1}$, 547.78 $cm^{-1,}$ and 480.28 $cm^{-1}$ attributed to the Fe bond vibration of BFFeNPs. A similar result was demonstrated by Wang et al. [47].

Fig. 2(d) shows the SEM images of bioflocculant mediated iron nanoparticles. It can be seen that the

obtained BFFeNPs have a spherical shape. Similar results have been reported for iron NPs prepared by different tea extracts and mint leaves extract [42, 45]. Moreover, the iron nanoparticles tended to aggregate probably due to the existence of polyphenols in the okra bioflocculant. Aggregation of the nanoparticles usually causes to increase in the size of nanoparticles, this is a common phenomenon during biosynthesis of metallic nanoparticles particularly when the plant extracts are used [48].

The elemental composition of the BFFeNPs was determined by the EDX. In the EDX spectrum (Fig. 2(e), three intense peaks of C, O, and Fe were found, which confirmed the formation of iron nanoparticles by okra-mediated bioflocculant. The presence of carbon and oxygen may arise from biomolecules of okra bioflocculant which was acted as a capping agent. Similar observations were also reported by Wang et al. for the synthesis of iron nanoparticles using eucalyptus leaves extracts. The presence of Fe (32.30%) demonstrated that iron nanoparticles have been synthesized. The weight composition of Fe synthesized by okra-mediated bioflocculant is relatively higher than that of eucalyptus leaf extract whose percentage reported to be 16.17% [47]. The weight percentages of C and O in the obtained product were 27.29 % and 40.41 %, respectively.

AFM analysis was also performed to evaluate the nature of BFFeNPs and the response is shown in Fig. 2(f). The surface topology of BFFeNPs can be accessed from the grooves present in the dimensional views of iron nanoparticles. From the 3D view, it is observed that the size of the nanoparticle was variables in size. This behavior was noted in the case of BFFeNPs because of the presence of various bioactive molecules. Since bioactive molecules have different functional groups, which interact with one other by intermolecular forces, the particle may hold together and particle size may vary [49].

The size of the synthesized BFFeNPs was illustrated in the TEM images as shown in Figs. 2 (g) and (h). The TEM micrograph illustrated that the okra bioflocculant mediated Fe nanoparticles exhibited spherical nanostructures with an average diameter of 50 nm (Fig. 2(h) and the particles were seen to be agglomerated (Fig. 2 (g). Similar results of TEM analysis were reported where electron-dense spherical iron oxide particles having a diameter ranging from 30 to 40 nm were synthesized using *Hordeum vulgare* extracts and *Rumex acetosa* extracts [50].

The DLS analysis of BFFeNPs showed an average particle size of 52 nm. Some of the nanoparticles have irregular shapes because of agglomeration. It is observed that most of the BFFeNPs are spherical. Similar results are reported by Karimi et al. [11].

*Flocculation assay using simulated wastewater containing heavy metals*

The flocculation efficiency was tested for the purified bioflocculant and BFFeNPs using a simulated waster containing heavy metals.

Fig. 3 showed that the removal of the heavy

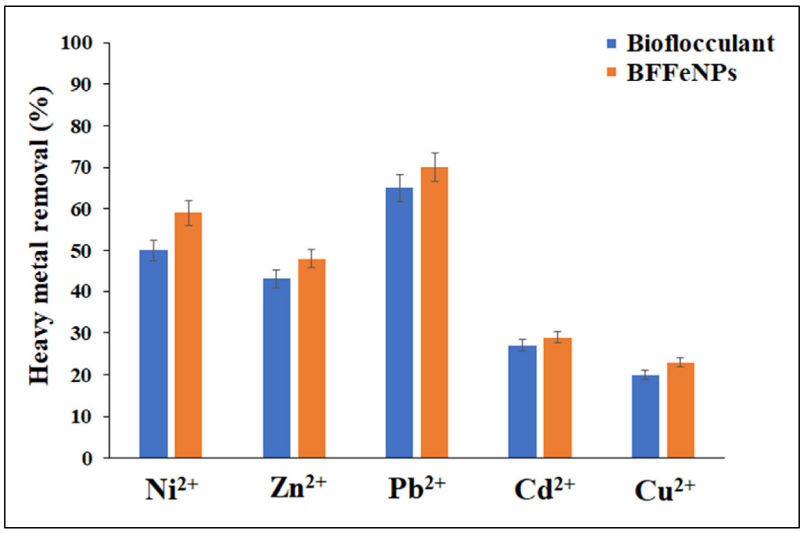


Fig. 3. Heavy metal removal from simulated wastewater.

Table 2. The percentage removal of heavy metals from real wastewater

| | Percentage Removal (%) | |
|---|---|---|
| **Heavy Metals** | **Bioflocculant** | **BFFeNPs** |
| $Pb^{2+}$ | 66.22 ± 0.22** | 70.14 ± 0.11** |
| $Ni^{2+}$ | 50.42 ± 0.31 | 60.69 ± 0.48 |
| $Zn^{2+}$ | 48.10 ± 0.13 | 50.22 ± 0.04 |
| $Cd^{2+}$ | 33.19 ± 0.08 | 45.64 ±0.47 |
| $Cu^{2+}$ | 30.68 ± 0.16 | 37.58 ± 0.28 |

** highest percent removal for each metal ($p<0.05$)

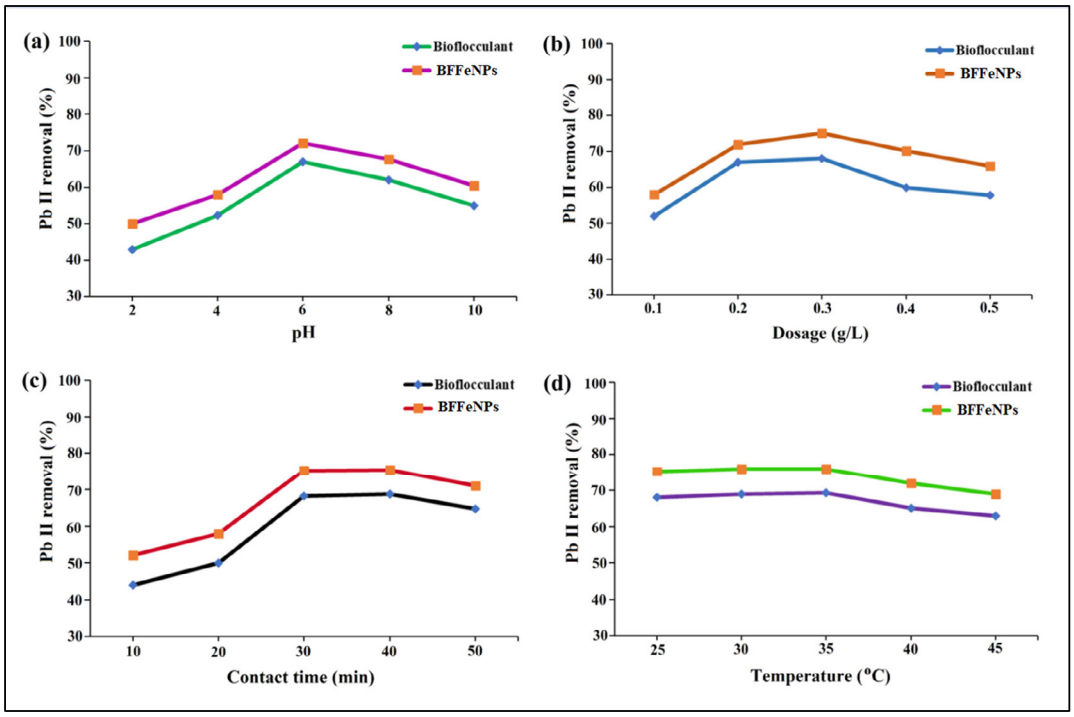


Fig. 4. Effect of parameters on Pb(II) removal from real wastewater using purified Okra bioflocculant and BFFeNPs (a) Effect of pH, (b) Effect of dosage, (c) Effect of contact time, and (d) Effect of temperature.

metals viz. $Ni^{2+,}$ $Zn^{2+}$, $Pb^{2+}$, $Cd^{2+}$ and $Cu^{2+}$ was found to be 50, 43, 65, 27 and 20 %, respectively using only bioflocculant. Compared to this, BFFeNPs was capable of removing $Ni^{2+,}$ $Zn^{2+}$, $Pb^{2+}$, $Cd^{2+}$ and $Cu^{2+}$ by 59, 48, 70, 29 and 23% respectively.

*Heavy metal removal from real wastewater using BFFeNPs*

The removal percentage of heavy metals viz. $Pb^{2+}$, $Ni^{2+}$, $Zn^{2+}$, $Cd^{2+}$ and $Cu^{2+}$ from wastewater are summarized in Table 2.

The $Pb^{2+}$ removal percentage of 66.22 % and 70.14% was recorded highest among all metals using Okra bioflocculant and BFFeNPs respectively. The results on heavy metal removal signify the efficiency of BFFeNPs which was more compared to the application of bioflocculant alone. Removal pattern followed was as follows : $Pb2^{+}$> $Ni^{2+}$> $Zn^{2+}$> $Cd^{2+}$> $Cu^{2+}$ in both the cases.

*Effect of parameters on Pb (II) removal*

The effect of pH was monitored in the range 2–10, keeping all other factors constant, that is bioflocculant and BFFeNPs dosage of 0.2 g/L, contact time (30 min), and temperature of 25°C. Fig. 4(a) shows the removal percentage of Pb (II) ions depends significantly on pH. The percentage removal gradually increased with an increase in pH up to pH 6; above this value, insoluble lead hydroxides were seen to precipitate out. The low metal removal at pH 2 was due to the excess $H^{+}$ ions and consequent protonation of BFFeNPs

surface [12]. At pH 4-6 phosphate, carboxyl, and amino groups on the okra bioflocculant and BFFeNPs generate a negatively charged surface and electrostatic interactions between cationic species and this surface can be responsible for enhanced lead removal. The maximum Pb (II) removal of 67% and 72.09% was achieved at pH 6 using okra bioflocculant and BFFeNPs respectively.

The experiment was carried out to determine the optimum dosage for Pb (II) removal at optimum pH of 6, contact time of 30 min, and temperature of 25°C. The bioflocculant and BFFeNPs dosage were varied in the range from 0.1-0.5 g/L. Fig. 4(b) shows that the Pb (II) removal percentage increased with an increase in dosage of bioflocculant and BFFeNPs up to the optimum level of 0.3 g/L after which a gradual decrease in Pb (II) removal percentage was observed. The number of active sites on bioflocculant and BFFeNPs will increase with increasing dosage, so, the binding chances of Pb (II) ion with bioflocculant and BFFeNPs surface increases and Pb (II) ion removal efficiency also increases [12]. It was observed that the synthesized iron nanoparticles have a high affinity than the bioflocculant for removal of Pb (II) ion with removal efficiency above 75 % at the dosage of 0.3 g/L. Similar results were reported by Dlamini et al. [17].

The contact time is another important parameter for the removal of Pb (II) ions. Fig. 4(c) shows the variation in Pb (II) removal with different contact times ranging from 10-50 min using 0.3 g/L of bioflocculant and BFFeNPs dosage at pH 6 and the temperature was fixed at 25 °C. The results for the effect of contact time on Pb (II) removal are represented in Fig. 4(c). It was observed that removal efficiency increased initially after that it became steady, denoting the attainment of equilibrium [51]. The reason for the short time equilibrium is the entire active sites of the bioflocculant and BFFeNPs were vacant at the beginning and the binding affinity of Pb (II) will increase towards these active sites [12]. At the equilibrium point, the highest Pb (II) removal efficiency of about 75.50% with BFFeNPs and 68.78 %with bioflocculant were obtained at 30 min of contact time.

Fig. 4(d) shows the effect of temperature on Pb (II) removal efficiency. The relationship between temperature and removal efficiency of BFFeNPs was examined at a temperature range from 25-50° C. As the temperature increased, the removal percentage of Pb (II) ion was also increased till it reached the optimum level. The highest removal efficiency of 76.14% was achieved at 35°C which was in good agreement with the result reported by Nharingo et al. [34].

*Process optimization for maximum removal of lead (II)*

Response surface methods were used to determine the effect of different variables such as pH (2, 4, 6, 8 and 10), BFFeNPs dosage (0.1, 0.2 and 0.3 g/L), contact time (10, 20, 30, 40 and 50 min) and temperature (10, 20, 30, 40 and 50 °C) on Pb (II) removal percentage. A quadratic model of three factorial BBD was selected for the optimization of variables. A total of 29 runs were conducted to get the best levels of variables. Four parameters (pH, BFFeNPs dosage, contact time, and temperature) were taken as independent variables and Pb (II) removal percentage was taken as a response to the study. The responses of predicted and experimental values were computed using Analysis of variance (ANOVA) to check whether the polynomial expression is able to predict the responses statistically (Table 3). The ANOVA for the quadratic model of response (Pb (II) removal) was tabulated in Table 3.

P-value (< 0.0001) obtained revealed the regression model is significant. F value (4780.74) obtained further implies that the model is highly significant for the removal of Pb (II). There is only a 0.01% chance that a large F value could occur due to noise. Values of "Prob>F" less than 0.0500 indicate that model terms are significant [52]. In this case, A, B, C, D, AB, BC, BD, CD, $A^2$, $B^2$, $C^2$, $D^2$ are the significant model terms. Lack of fit F value-0.0446 implies a non-significant lack of fit. The goodness of the model was restricted by $R^2$ (coefficient of determination). The high $R^2$ value (0.9998) obtained is very close to 1.0 and advocates a great correlation between the predicted and actual values. The value of Predicted $R^2$ (0.9996) and Adjusted $R^2$ (0.9996) are in reasonable agreement. The regression model selected provides a clear explanation of the relationship between the variables and response. The relationship between the selected variables and response (Pb II removal) for the quadratic model was demonstrated by the second-order polynomial equation:

Response: Pb II removal ($Y_{Pb\ II}$) = + 91.46 + 0.8783 × A + 1.81 × B + 0.2833 × C – 0.8017 × D – 2.20 ×

Table 3. ANOVA for response surface quadratic model (Response Pb II % removal)

| Source | Sum of Squares | df | Mean Square | F-value | p-value | |
|---|---|---|---|---|---|---|
| Model | 5214.25 | 14 | 372.45 | 4780.74 | < 0.0001 | *** |
| A-pH | 9.26 | 1 | 9.26 | 118.83 | < 0.0001 | *** |
| B-BFFeNPs dosage | 39.39 | 1 | 39.39 | 505.56 | < 0.0001 | *** |
| C-Contact time | 0.9633 | 1 | 0.9633 | 12.37 | 0.0034 | ** |
| D-Temperature | 7.71 | 1 | 7.71 | 98.99 | < 0.0001 | *** |
| AB | 19.45 | 1 | 19.45 | 249.64 | < 0.0001 | *** |
| AC | 0.0784 | 1 | 0.0784 | 1.01 | 0.3328 | NS |
| AD | 23.33 | 1 | 23.33 | 299.45 | < 0.0001 | *** |
| BC | 19.45 | 1 | 19.45 | 249.64 | < 0.0001 | *** |
| BD | 30.58 | 1 | 30.58 | 392.54 | < 0.0001 | *** |
| CD | 1.93 | 1 | 1.93 | 24.80 | 0.0002 | ** |
| $A^2$ | 4240.97 | 1 | 4240.97 | 54437.23 | < 0.0001 | *** |
| $B^2$ | 924.71 | 1 | 924.71 | 11869.62 | < 0.0001 | *** |
| $C^2$ | 765.69 | 1 | 765.69 | 9828.48 | < 0.0001 | *** |
| $D^2$ | 1155.14 | 1 | 1155.14 | 14827.45 | < 0.0001 | *** |
| Residual | 1.09 | 14 | 0.0779 | | | |
| Lack of Fit | 0.1094 | 10 | 0.0109 | 0.0446 | 0.9999 | NS |
| Pure Error | 0.9813 | 4 | 0.2453 | | | |
| Cor Total | 5215.35 | 28 | | | | |
| Std. Dev. | 0.2791 | | | | | |
| Mean | 65.92 | | | | | |
| C.V. % | 0.4234 | | | | | |
| $R^2$ | 0.9998 | | | | | |
| Adjusted $R^2$ | 0.9996 | | | | | |
| Predicted $R^2$ | 0.9996 | | | | | |
| Adeq Precision | 211.2430 | | | | | |

***Highly significant (p-value< 0.0001); **Significant (p-value <0.005); NS, Non-significant (p-value> 0.005).

$AB - 0.1400 \times AC - 2.41 \times AD + 2.21 \times BC + 2.76 \times BD - 0.6950 \times CD - 25.57 \times A^2 - 11.94 \times B^2 - 10.86 \times C^2 - 13.34 \times D^2$.

Where ($Y_{Pb\ II}$) represents Pb (II) removal (%) as response and A, B, C and D were coded terms for the four test variables i.e., pH, BFFeNPs dosage, contact time, and temperature respectively. The 3-dimensional (3D) and 2-dimensional (2D) contour plots showed a significant influence on the response using BFFeNPs. The 3D and 2D contour plots are helpful to investigate the interactive effect of two variables on Pb(II) removal percent in the experimental ranges as given in Figs. 5, 6, and 7.

3D and 2D Contour plots were shown in Fig. 5(a) illustrating the interactive effect of pH and BFFeNPs dosage on Pb (II) removal (%). As indicated in the figures., after optimum level Pb (II) removal percent was increased with an increase in the pH of the wastewater. Maximum Pb II removal percentage was achieved at pH 6 with a Pb (II) removal efficiency of 91.45%. Similar results regarding optimum pH of Pb (II) removal by fungal biomass were reported by Amin et al.[45]. According to Nharingo et al. at acidic pH, there is competition between hydrogen ($H^+$) ions and the metal ions for the negatively charged sites on the anionic BFFeNPs. The minimum Pb (II) percentage removal was observed at acidic pH (1-5) due to repulsion between protonated BFFeNPs and the positive Pb (II) ions. The diminishing levels of $H^+$ ions in solution, as pH was increased, gave rise to Pb (II) ions being the central cationic species in solution; hence, its percentage removal increased with pH. As pH increased the enhancement of metal flocculation was observed this is due to the high electrostatic attraction between negatively charged sites of BFFeNPs and the positively charged Pb (II) ions [34]. At alkaline pH (7-10), the Pb (II) removal percentage remained constant. A similar trend of results was illustrated by Dlamini et al. [17]. At higher pH than the optimum level, flocculation may be hindered by the formation of hydroxo species of metal ion that do not bind to the BFFeNPs. Furthermore, the availability of the positively charged and negatively charged site fluctuates with pH, with the latter commonly decreased with increasing pH than the optimal

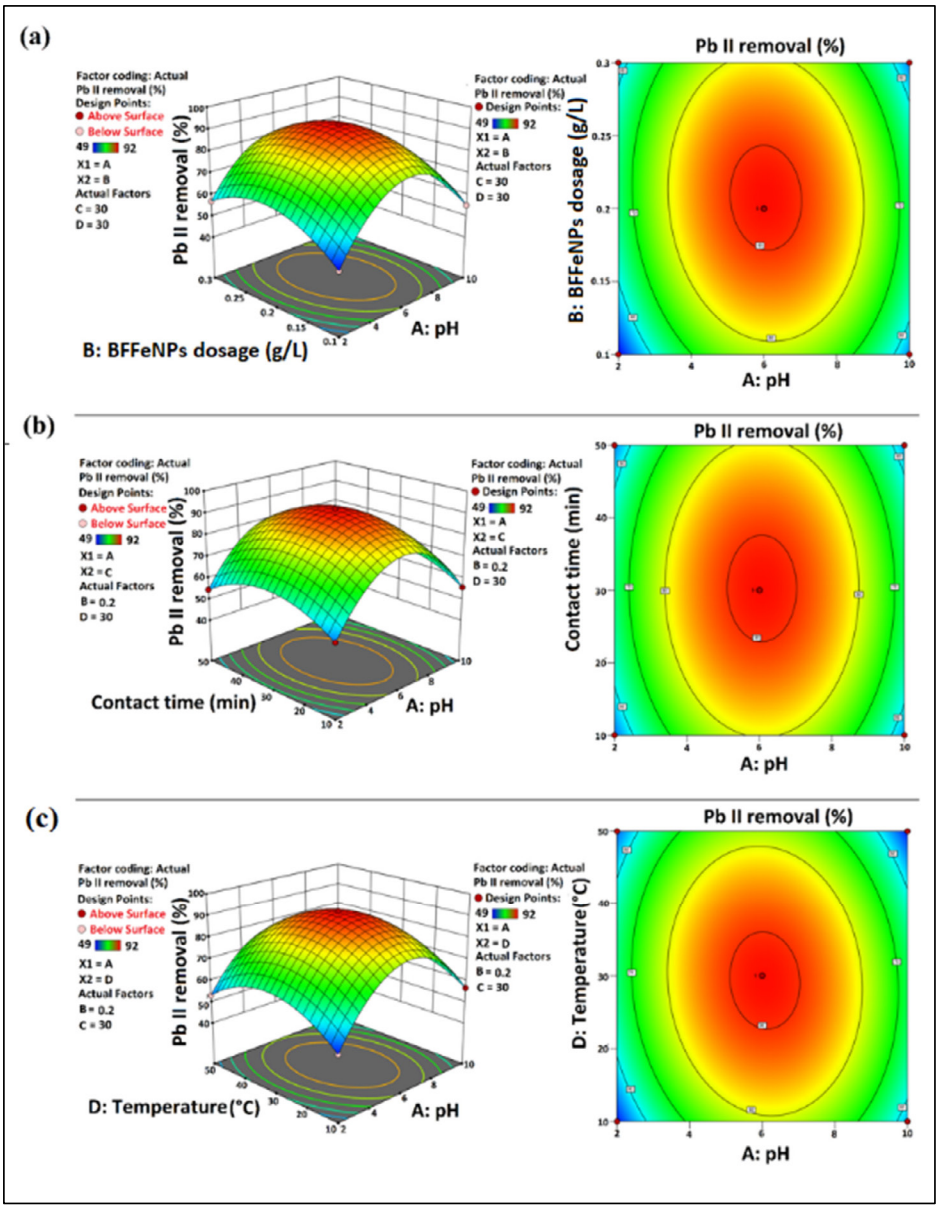


Fig. 5. Response surface 3D and contour plots showing the interactive effect between (a) pH and BFFeNPs dosage (AB), (b) pH and Contact time (AC), (c) pH and temperature (AD) during Pb (II) removal.

level, thus resulting in a lower metal removal at higher pH through bioflocculation [33].

While in the case of BFFeNPs dosage, a gradual increase in Pb (II) removal (%) with an increase in BFFeNPs dosage was observed. An increase in dosage increased to negatively charged sites available for Pb (II) ion aggregation. A similar trend was observed for the biocoagulation-flocculation of Pb (II) ion from wastewater using cactus *Opuntia ficus indica* [34]. After the optimum level, a further increase in dosage causes the re-spreading of aggregated particles and also disturbs particle settling. Above the optimum dosage of 0.2 g/L, the trends showed a decrease in removal percentage due to some steric repulsion attributed to particle stabilization. Thus, removal efficiency decreases with increasing dosage beyond the optimum [34]. The BFFeNPs dosage of 0.2 g/L brought about complete charge neutralization of the Pb (II) ion and was therefore identified as the optimum dosage for the removal of Pb (II) ions from wastewater.

The interactive effect of pH and contact time

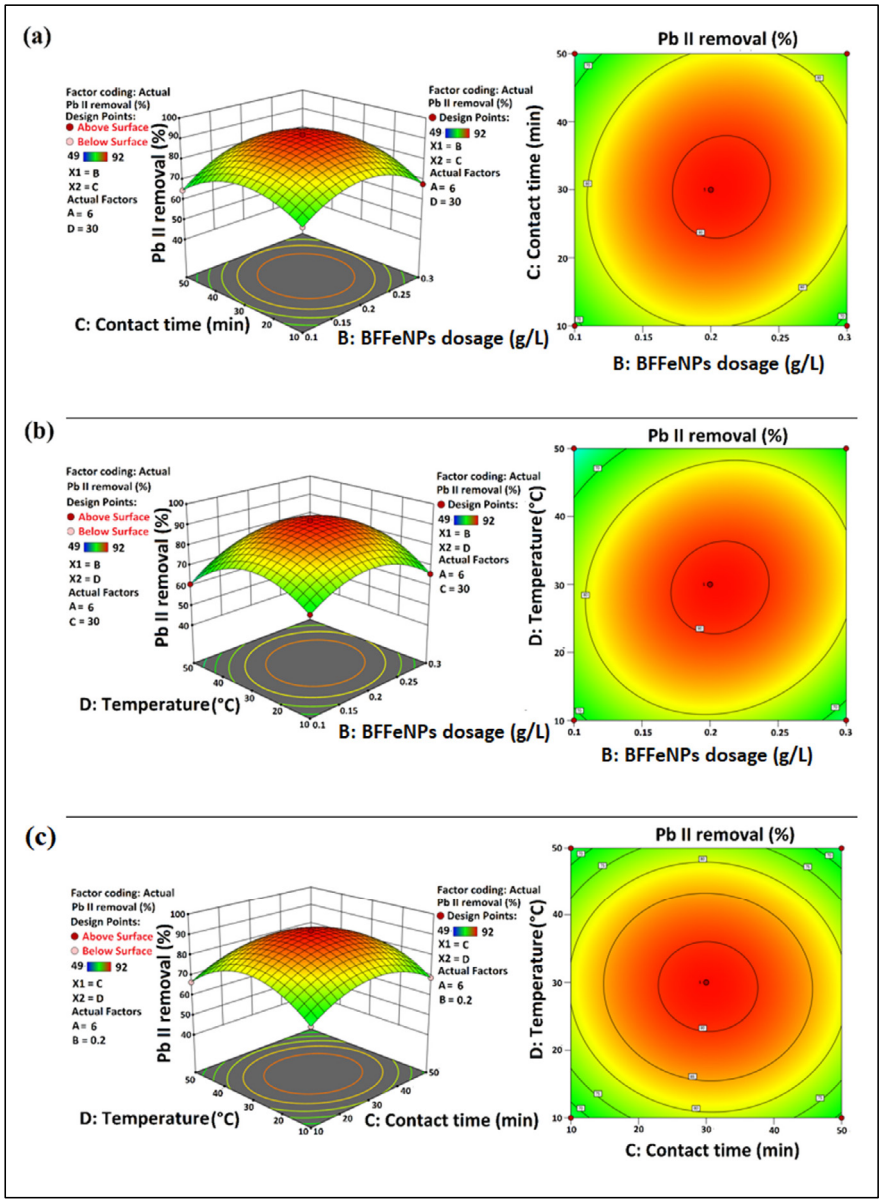


Fig. 6. Response surface 3D and contour plots showing the interactive effect between (a) BFFeNPs dosage and contact time (BC), (b) BFFeNPs dosage and temperature (BD) and (c) contact time and temperature (CD) during Pb (II) removal.

on Pb (II) removal percentage was shown by 3D surface graphs and 2D contour plots Fig. 5(b). As contact time increases, the Pb (II) removal (%) also increases up to the optimum level. The highest Pb (II) removal (%) was observed at 30 min of contact time, after which no significant increase in removal percent was observed.

Fig. 5(c) shows the interactive effect of pH and temperature. Maximum Pb (II) removal was obtained at pH 6 and temperature 30°C. Coagulation-flocculation is affected by higher temperatures. Temperature beyond the optimum level results in rapid movement of particles that disturb their agglomeration; hence minimum removal of metal ions occurs [53].

As seen in Fig. 6(a), it is evident from the graphs that both the variables (BFFeNPs dosage and contact time) strongly influenced the Pb (II) removal response. Maximum Pb(II) removal was achieved at 0.2 g/L of BFFeNPs dosage and contact time 30 min. After the optimum level of dosage and contact time, Pb (II) removal percentages

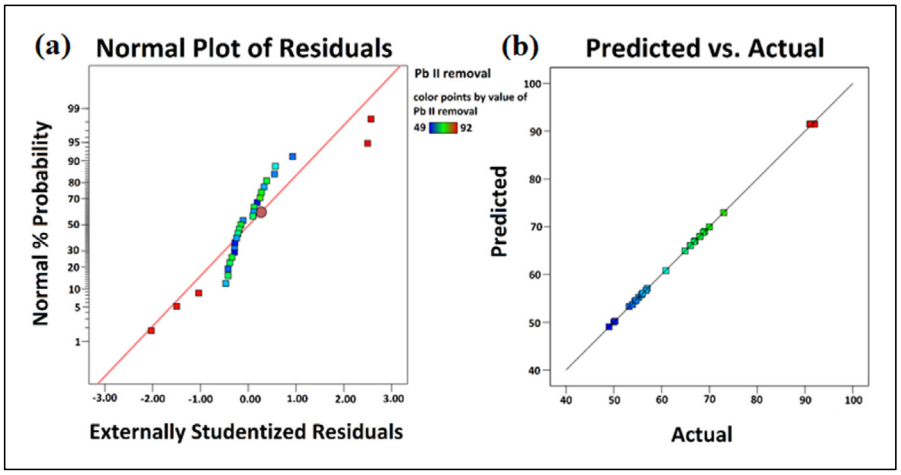


Fig. 7. (a) Normal plot of residuals and (b) predicted vs. actual plot.

Table 4. Actual versus predicted value for Response (Pb II removal (%)

| Run Order | pH | BFFeNPs dosage (g/L) | Contact time (min) | Temperature (°C) | Response (Pb II removal (%) | |
|---|---|---|---|---|---|---|
| | | | | | Actual value | Predicted value |
| 1 | 2 | 0.2 | 30 | 10 | 50.00 | 50.05 |
| 2 | 6 | 0.2 | 10 | 50 | 66.78 | 66.86 |
| 3 | 2 | 0.2 | 50 | 30 | 54.67 | 54.57 |
| 4 | 10 | 0.3 | 30 | 30 | 54.38 | 54.43 |
| 5 | 2 | 0.2 | 30 | 50 | 53.20 | 53.28 |
| 6 | 6 | 0.1 | 30 | 10 | 68.00 | 67.93 |
| 7 | 6 | 0.2 | 30 | 30 | 92.00 | 91.46 |
| 8 | 10 | 0.2 | 30 | 50 | 50.24 | 50.20 |
| 9 | 6 | 0.2 | 30 | 30 | 91.10 | 91.46 |
| 10 | 10 | 0.1 | 30 | 30 | 55.20 | 55.22 |
| 11 | 6 | 0.3 | 30 | 50 | 70.00 | 69.95 |
| 12 | 6 | 0.3 | 10 | 30 | 68.00 | 67.98 |
| 13 | 6 | 0.2 | 30 | 30 | 91.99 | 91.46 |
| 14 | 6 | 0.3 | 50 | 30 | 73.00 | 72.95 |
| 15 | 6 | 0.1 | 50 | 30 | 64.88 | 64.92 |
| 16 | 10 | 0.2 | 30 | 10 | 56.70 | 56.64 |
| 17 | 6 | 0.2 | 30 | 30 | 91.00 | 91.46 |
| 18 | 6 | 0.1 | 30 | 50 | 60.90 | 60.80 |
| 19 | 2 | 0.2 | 10 | 30 | 53.89 | 53.72 |
| 20 | 6 | 0.3 | 30 | 10 | 66.04 | 66.02 |
| 21 | 6 | 0.2 | 50 | 10 | 69.00 | 69.03 |
| 22 | 6 | 0.2 | 10 | 10 | 67.00 | 67.07 |
| 23 | 10 | 0.2 | 50 | 30 | 56.00 | 56.05 |
| 24 | 6 | 0.2 | 50 | 50 | 66.00 | 66.03 |
| 25 | 6 | 0.1 | 10 | 30 | 68.70 | 68.76 |
| 26 | 6 | 0.2 | 30 | 30 | 91.20 | 91.46 |
| 27 | 10 | 0.2 | 10 | 30 | 55.78 | 55.76 |
| 28 | 2 | 0.3 | 30 | 30 | 57.00 | 57.09 |
| 29 | 2 | 0.1 | 30 | 30 | 49.00 | 49.05 |

were slower because the active sites of BFFeNPs and bioflocculant are occupied by Pb (II) ions. Similar findings for Pb II removal were reported by Celebi& Gök [51].

BFFeNPs dosage and temperature also influenced the removal of Pb (II) ions. Fig. 6(b) depicts the interactive effect of BFFeNPs dosage and temperature. Highest Pb (II) removal percentage was observed at 0.2 g/L of BFFeN dosage and 30°C of temperature. Fig. 6(c) shows the effect of contact time and temperature on Pb (II) removal (%).

The expected values of Pb (II) removal

percentage were calculated by regression analysis and correlated to the actual data which demonstrated that the experimental response values were in good agreement with the expected (predicted) response values (Table 4).

The normal plot for residuals and predicted vs actual plots of the Pb (II) removal (%) (response), were presented in Fig. 7 (a) and Fig. 7 (b) respectively.

A statistical design was confirmed by implementing a point prediction tool of RSM from an optimal value of all the four factors A, B, C, and D which were used for the experiment. The optimized factors of the Pb (II) removal percentage attained were A: pH (6), B: BFFeNPs dosage (0.2 g/L), C: contact time (30 min), and D: temperature (30°C). The experimental Pb (II) removal percentage (91.45±0.49%) was in good agreement with the predicted value (91.46±0.1%) demonstrating the rationality of the design. Thus, a significant increase in the Pb (II) removal percentage from 76.14 to 91.45% was attained using BFFeNPs under optimized conditions.

A comparison was carried out of the adsorption efficiency for Pb (II) ions removal by other adsorbents with current synthesized BFFeNPs nanoparticles and is shown in Table 5 [12, 52, 53, 54]. The adsorption efficiency within a short contact time and low BFFeNPs dosage of this study revealed that bioflocculant mediated iron nanoparticles (BFFeNPs) could be a promising adsorbent for Pb (II) ions removal.

*Adsorbent recovery*

Regeneration of adsorbent is one of the key steps in the adsorbent economy for further uses to keep the process cost-effective. In the first step of the desorption process for Pb (II), the metal ions adsorbed iron nanoparticles were washed with distilled water to remove the unabsorbed Pb (II) ions which were loosely attached to the BFFeNPs adsorbent. Then, the BFFeNPs adsorbent was separated by centrifugation (at 6000 rpm for 5 min) and was shaken with 50 ml of 0.2M HCl. Thereafter, the remained solution was analyzed utilizing the atomic absorption spectrophotometer and the separated sorbents were washed with distilled water. Finally, the recovered BFFeNPs adsorbent was dried at 120 °C for 60 min. [57].

The metal recovery was calculated by the following equation :

$$\text{Recovery (\%)} = \frac{\text{Amount of desorbed metals}}{\text{Amount of adsorbed metals}} \times 100$$

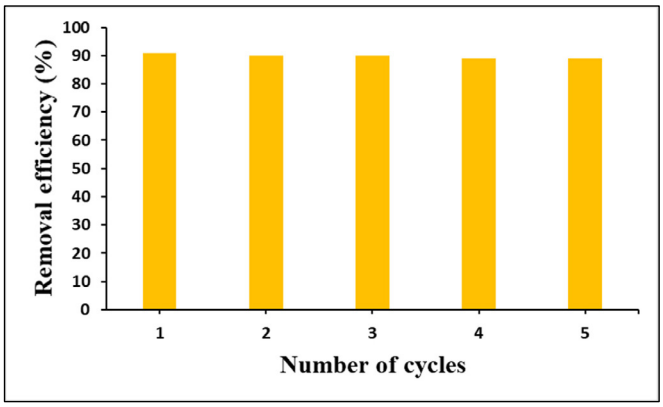


Fig. 8. The removal of Pb (II) ion by recycled BFFeNPs.

Table 5. The comparison of Pb (II) removal efficiency for different adsorbent

| Adsorbent | PB (II) removal efficiency | References |
|---|---|---|
| BFFeNPs | 91.45% | Present study |
| FeNi3@SiO2 magnetic nano-composite | 87.31% | [12] |
| $TiO_2$ NPs | 82.53% | [54] |
| Zinc Oxide Nanoparticles | 93% | [55] |
| CuO nanoparticles | 76.5% | [56] |

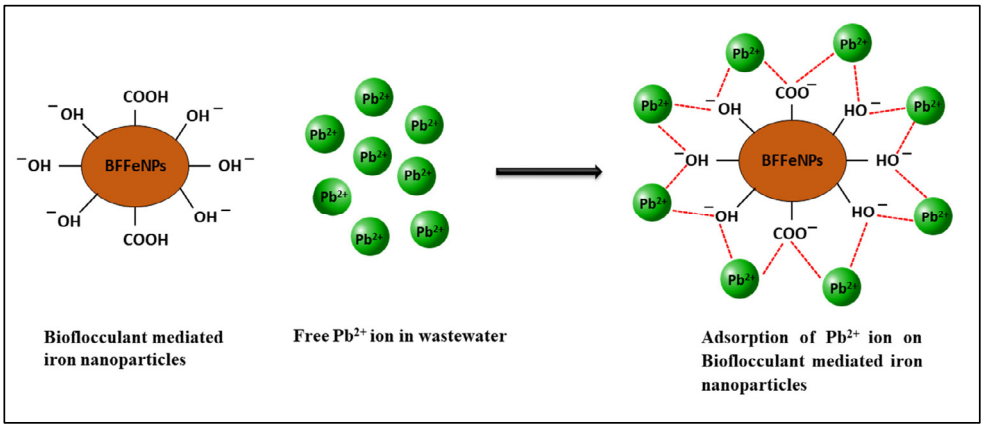


Fig. 9. Schematic representation of the possible mechanism of Pb (II) ion adsorption on BFFeNPs.

In the present study, BFFeNPs adsorbents desorbed ~89% of the adsorbed Pb (II). Fig. 8. This showed that there was no significant change in desorption efficiencies, even after five cycles. These results showed that BFFeNPs is potential adsorbent with high adsorption and desorption capabilities.

*Mechanism of lead (II) adsorption*

The proposed mechanism for Pb (II) ion adsorption onto BFFeNPs is illustrated in Fig. 9. It can be concluded that BFFeNPs removes Pb (II) ion by the following strategies 1) Pb (II) exists in wastewater as cations that can be removed via electrostatic force of attraction 2) Pb (II) interact more specifically with the functional groups on the surface of BFFeNPs [58].

The presence of functional groups such as the COOH group of conjugated carbonyls (mainly ketones and esters) and polar groups on the BFFeNPs surface that was shown by the FTIR analysis is responsible for the chemical adsorption of Pb (II) ion [59]. There are a large number of –OH functional groups on BFFeNPs. At low pH conditions, the number of $H^+$ ions in the wastewater sample increases, and –OH groups become positively charged $–OH^{2+}$, decreasing the adsorption capability of Pb(II) ions on the surface of the BFFeNPs adsorbent. At pH values higher than 6, there will be a decrease in adsorption of Pb (II) ion due to precipitation of Pb (II) in the form of $Pb(OH)_2$ [60].

## CONCLUSIONS

In this study, bioflocculant mediated iron nanoparticles (BFFeNPs) was utilized for the successful removal of Pb (II) ion from the wastewater within a short contact time. Continuous adsorption in the range of 200-350 nm in UV-Visible spectra indicated the existence of iron nanoparticles. The BFFeNPs was synthesized and characterized by different instrumental analysis (UV, XRD, FTIR, SEM, EDX, TEM, DLS, and AFM). SEM and TEM analysis exhibited that the synthesized Fe nanoparticles have a spherical shape. DLS analysis revealed an average particle diameter of 52 nm. In addition, response surface methodology was adopted for statistical optimization using BBD to enhance the Pb (II) removal efficiency. Optimum values obtained were pH 6.0, BFFeNPs dosage 0.2 g/L, contact time 30 min and temperature30°C. Flocculation activity was increased up to 91% after process optimization. This result showed that bioflocculant mediated iron nanoparticles (BFFeNPs) could be utilized as an efficient, cost-effective flocculant for bioremediation of Pb (II) ions from wastewater.

## ACKNOWLEDGEMENTS

This study was funded by University Grants Commission, India, grant (800/(CSIR-UGC NET DEC. 2017), New Delhi, India Authors are thankful to the School of Advanced Sciences (SAS), School of Bio-Medical Sciences (SBST), and DST-FIST/ VIT SEM of Vellore Institute of Technology, India for providing laboratory facilities while conducting the experimental work.

## CONFLICT OF INTEREST

The authors declare no conflict of interest.

## REFERENCES

1. Thakkar KN, Mhatre SS, Parikh RY. Biological synthesis of metallic nanoparticles. Nanomedicine: Nanotechnology, Biology and Medicine. 2010;6(2):257-62.
2. Muthulakshmi L, Rajini N, Varada Rajalu A, Siengchin S,

Kathiresan T. Synthesis and characterization of cellulose/ silver nanocomposites from bioflocculant reducing agent. International Journal of Biological Macromolecules. 2017;103:1113-20.
3. Daphne J, Francis A, Mohanty R, Ojha N, Das N. Green Synthesis of Antibacterial Silver Nanoparticles using Yeast Isolates and its Characterization. Research Journal of Pharmacy and Technology. 2018;11(1):83.
4. Bose D, Chatterjee S. Biogenic synthesis of silver nanoparticles using guava (Psidium guajava) leaf extract and its antibacterial activity against Pseudomonas aeruginosa. Applied Nanoscience. 2015;6(6):895-901.
5. Sayadi MH, Salmani N, Heidari A, Rezaei MR. Bio-synthesis of palladium nanoparticle using Spirulina platensis alga extract and its application as adsorbent. Surfaces and Interfaces. 2018;10:136-43.
6.Yazdani A, Sayadi M, Heidari A. Green biosynthesis of palladium oxide nanoparticles using *Dictyota indica* seaweed and its application for adsorption. Journal of Water and Environmental Nanotechnology. 2018; 3(4):337-47.
7. Fujita M, Ide Y, Sato D, Kench PS, Kuwahara Y, Yokoki H, et al. Heavy metal contamination of coastal lagoon sediments: Fongafale Islet, Funafuti Atoll, Tuvalu. Chemosphere. 2014;95:628-34.
8. Al-Gheethi AA, Mohamed RMSR, Efaq AN, Norli I, Abd Halid A, Amir HK, et al. Bioaugmentation process of secondary effluents for reduction of pathogens, heavy metals and antibiotics. Journal of Water and Health. 2016;14(5):780-95.
9. Hua M, Zhang S, Pan B, Zhang W, Lv L, Zhang Q. Heavy metal removal from water/wastewater by nanosized metal oxides: A review. Journal of Hazardous Materials. 2012;211-212:317-31.
10.Xu P, Zeng GM, Huang DL, Feng CL, Hu S, Zhao MH, Liu ZF. Use of iron oxide nanomaterials in wastewater treatment: a review. Science of the Total Environment, 2012; 424:1-10.
11. Karimi, Javanshir, Sayadi, Arabyarmohammadi. Arsenic Removal from Mining Effluents Using Plant-Mediated, Green-Synthesized Iron Nanoparticles. Processes. 2019;7(10):759.
12. Farooghi A, Sayadi MH, Rezaei MR, Allahresani A. An efficient removal of lead from aqueous solutions using FeNi 3 @SiO 2 magnetic nanocomposite. Surfaces and Interfaces. 2018;10:58-64.
13. Hosseini R, Sayadi MH, Shekari H. Adsorption of Nickel and Chromium From Aqueous Solutions Using Copper Oxide Nanoparticles: Adsorption Isotherms, Kinetic Modeling, and Thermodynamic Studies. Avicenna Journal of Environmental Health Engineering. 2019;6(2):66-74.
14. Ergüvenerler F, Targan Ş, Tirtom VN. Removal of lead from aqueous solutions by low cost and waste biosorbents (lemon, bean and artichoke shells). Water Science and Technology. 2020;81(1):159-69.
15. Shahadat M, Teng TT, Rafatullah M, Shaikh ZA, Sreekrishnan TR, Ali SW. Bacterial bioflocculants: A review of recent advances and perspectives. Chemical Engineering Journal. 2017;328:1139-52.
16. Lee D-J, Chang Y-R. Bioflocculants from isolated stains: A research update. Journal of the Taiwan Institute of Chemical Engineers. 2018;87:211-5.
17. Dlamini NG, Basson AK, Pullabhotla VSR. Optimization and Application of Bioflocculant Passivated Copper Nanoparticles in the Wastewater Treatment. Int J Environ Res Public Health. 2019;16(12):2185.
18. Karthiga devi K, Natarajan KA. Production and characterization of bioflocculants for mineral processing applications. International Journal of Mineral Processing. 2015;137:15-25.
19. Fan H-c, Yu J, Chen R-p, Yu L. Preparation of a bioflocculant by using acetonitrile as sole nitrogen source and its application in heavy metals removal. Journal of Hazardous Materials. 2019;363:242-7.
20. Can MM, Coşkun M, Fırat T. A comparative study of nanosized iron oxide particles; magnetite (Fe3O4), maghemite (γ-Fe2O3) and hematite (α-Fe2O3), using ferromagnetic resonance. Journal of Alloys and Compounds. 2012;542:241-7.
21. Abegunde SM, Idowu KS, Sulaimon AO. Plant-Mediated Iron Nanoparticles and their Applications as Adsorbents for Water Treatment–A Review. Journal of Chemical Reviews. 2020;2(2):103-13.
22.APHA1995 Standard methods for the examination of water and waste water, 19th edn. NewYork, USA.
23. Ameena K, Dilip C, Saraswathi R, Krishnan PN, Sankar C, Simi SP. Isolation of the mucilages from Hibiscus rosasinensis linn. and Okra (Abelmoschus esculentus linn.) and studies of the binding effects of the mucilages. Asian Pacific Journal of Tropical Medicine. 2010;3(7):539-43.
24. Nielsen SS. Phenol-Sulfuric Acid Method for Total Carbohydrates. Food Analysis Laboratory Manual: Springer US; 2009. p. 47-53.
25. Bradford MM. A rapid and sensitive method for the quantitation of microgram quantities of protein utilizing the principle of protein-dye binding. Analytical Biochemistry. 1976;72(1-2):248-54.
26.Zhang W. 2003 Biological-chemical analysis of Glycoconjugates, 2nd edn. Zhejiang University Press, Zhejiang.
27. Eman Zakaria G. Production and Characteristics of a Heavy Metals Removing Bioflocculant Produced by Pseudomonas aeruginosa. Polish Journal of Microbiology. 2012;61(4):281-9.
28. Rasulov BA, Pattaeva MA, Yili A, Aisa HA. Polysaccharide-based bioflocculant template of a diazotrophic Bradyrhizobium japonicum 36 for controlled assembly of AgCl nanoparticles. International Journal of Biological Macromolecules. 2016;89:682-8.
29. Saravanan C, Rajesh R, Kaviarasan T, Muthukumar K, Kavitake D, Shetty PH. Synthesis of silver nanoparticles using bacterial exopolysaccharide and its application for degradation of azo-dyes. Biotechnol Rep (Amst). 2017;15:33-40.
30. Prasad KS, Gandhi P, Selvaraj K. Synthesis of green nano iron particles (GnIP) and their application in adsorptive removal of As(III) and As(V) from aqueous solution. Applied Surface Science. 2014;317:1052-9.
31.Jeyasundari J, Praba PS, Jacob YB, Vasantha VS, Shanmugaiah V. Green synthesis and characterization of zero valent iron nanoparticles from the leaf extract of *Psidium guajava* plant and their antibacterial activity. Chemical Science Review and Letters. 2017; 6:1244-52.
32. Vitta Y, Figueroa M, Calderon M, Ciangherotti C. Synthesis of iron nanoparticles from aqueous extract of Eucalyptus robusta Sm and evaluation of antioxidant and antimicrobial activity. Materials Science for Energy Technologies. 2020;3:97-103.
33.Dih CC, Jamaluddin NA, Zulkeflee Z. Removal of heavy

metals in lake water using bioflocculant produced by *Bacillus subtilis*. Pertanika Journal of Tropical Agricultural Science. 2019; 42:89-101.
34. Nharingo T, Zivurawa MT, Guyo U. Exploring the use of cactus Opuntia ficus indica in the biocoagulation–flocculation of Pb(II) ions from wastewaters. International Journal of Environmental Science and Technology. 2015;12(12):3791-802.
35. Salehizadeh H, Shojaosadati SA. Removal of metal ions from aqueous solution by polysaccharide produced from Bacillus firmus. Water Research. 2003;37(17):4231-5.
36. Assi O, Sidibé D, Kouakou P, Deigna-Mockey V, Konan Y, Coulibaly A, et al. Characterization of the Mucilages of Four Food Plants, Abelmoschus esculentus, Beilschmiedia mannii, Corchorus olitorius, and Irvingia gabonensis, from Côte d'Ivoire. Biotechnology Journal International. 2017;19(2):1-10.
37.Acikgoz C, Borazan AA, Andoglu EM, Gokdai D. Chemical composition of Turkish okra seeds (*Hibiscus esculenta* L.) and the total phenolic contents of okra seeds. Applied Sciences & Engineering. 2016; 17:766-74.
38. Freitas TKFS, Oliveira VM, de Souza MTF, Geraldino HCL, Almeida VC, Fávaro SL, et al. Optimization of coagulation-flocculation process for treatment of industrial textile wastewater using okra (A. esculentus) mucilage as natural coagulant. Industrial Crops and Products. 2015;76:538-44.
39. swelam a-e, saied s, hafez A. "Removal comparative study for Cd(II) ions from polluted solutions by adsorption and coagulation techniques using Moringa Oleifera seeds". Egyptian Journal of Chemistry. 2019;0(0):0-.
40.Emeje M, Isimi C, Byrn S, Fortunak J, Kunle O, Ofoefule S. Extraction and physicochemical characterization of a new polysaccharide obtained from the fresh fruits of *Abelmoschus esculentus*. Iranian journal of pharmaceutical research. 2011; 10:237-46.
41. Zhang W, Xiang Q, Zhao J, Mao G, Feng W, Chen Y, et al. Purification, structural elucidation and physicochemical properties of a polysaccharide from Abelmoschus esculentus L (okra) flowers. International Journal of Biological Macromolecules. 2020;155:740-50.
42. Huang L, Weng X, Chen Z, Megharaj M, Naidu R. Green synthesis of iron nanoparticles by various tea extracts: Comparative study of the reactivity. Spectrochimica Acta Part A: Molecular and Biomolecular Spectroscopy. 2014;130:295-301.
43. Dhuper S, Panda D, Nayak PL. Green synthesis and characterization of zero valent iron nanoparticles from the leaf extract of *Mangifera indica*. Nano Trends: A Journal of Nanotechnology and Its Applications. 2012; 13:16-22.
44. Devatha CP, Thalla AK, Katte SY. Green synthesis of iron nanoparticles using different leaf extracts for treatment of domestic waste water. Journal of Cleaner Production. 2016;139:1425-35.
45. Ojha N, Mandal SK, Das N. Enhanced degradation of indeno(1,2,3-cd)pyrene using Candida tropicalis NN4 in presence of iron nanoparticles and produced biosurfactant: a statistical approach. 3 Biotech. 2019;9(3):86-.
46. Lotfi S, Aslibeiki B, Zarei M. Efficient Pb (II) removal from wastewater by TEG coated Fe3O4 ferrofluid. Journal of Water and Environmental Nanotechnology. 2021; 6:109-20.
47. Wang T, Jin X, Chen Z, Megharaj M, Naidu R. Green synthesis of Fe nanoparticles using eucalyptus leaf extracts for treatment of eutrophic wastewater. Science of The Total Environment. 2014;466-467:210-3.
48. Zangeneh MM, Zangeneh A. Biosynthesis of iron nanoparticles using Allium eriophyllum Boiss extract: Chemical characterization, antioxidant, cytotoxicity, antibacterial, antifungal, and cutaneous wound healing effects. Applied Organometallic Chemistry. 2019;34(1).
49.Bibi I, Nazar N, Ata S, Sultan M, Ali A, Abbas A, Jilani K, Kamal S, Sarim FM, Khan MI, Jalal F.Green synthesis of iron oxide nanoparticles using pomegranate seeds extract and photocatalytic activity evaluation for the degradation of textile dye. Journal of Materials Research and Technology. 2019; 8:6115-24.
50. Makarov VV, Makarova SS, Love AJ, Sinitsyna OV, Dudnik AO, Yaminsky IV, et al. Biosynthesis of Stable Iron Oxide Nanoparticles in Aqueous Extracts of Hordeum vulgare and Rumex acetosa Plants. Langmuir. 2014;30(20):5982-8.
51. Çelebi H, Gök O. Evaluation of Lead Adsorption Kinetics and Isotherms from Aqueous Solution Using Natural Walnut Shell. International Journal of Environmental Research. 2017;11(1):83-90.
52. Manohari, Singh J, Kadapakkam Nandabalan Y. Copper(II) Bioremoval by a Rhizosphere Bacterium, Stenotrophomonas acidaminiphila MYS1-Process Optimization by RSM Using Box–Behnken Design. International Journal of Environmental Research. 2017;11(1):63-70.
53. Amin F, Talpur FN, Balouch A, Afridi HI. Eco-efficient Fungal Biomass for the Removal of Pb(II) Ions from Water System: A Sorption Process and Mechanism. International Journal of Environmental Research. 2017;11(3):315-25.
54. Sethy NK, Arif Z, Mishra PK, Kumar P. Green synthesis of TiO2 nanoparticles from Syzygium cumini extract for photo-catalytic removal of lead (Pb) in explosive industrial wastewater. Green Processing and Synthesis. 2020;9(1):171-81.
55. Azizi S, Mahdavi Shahri M, Mohamad R. Green Synthesis of Zinc Oxide Nanoparticles for Enhanced Adsorption of Lead Ions from Aqueous Solutions: Equilibrium, Kinetic and Thermodynamic Studies. Molecules. 2017;22(6):831.
56. Verma M, Tyagi I, Chandra R, Gupta VK. Adsorptive removal of Pb (II) ions from aqueous solution using CuO nanoparticles synthesized by sputtering method. Journal of Molecular Liquids. 2017;225:936-44.
57. Tabesh S, Davar F, Loghman-Estarki MR. Preparation of γ-Al2O3 nanoparticles using modified sol-gel method and its use for the adsorption of lead and cadmium ions. Journal of Alloys and Compounds. 2018;730:441-9.
58. Lin Z, Weng X, Owens G, Chen Z. Simultaneous removal of Pb(II) and rifampicin from wastewater by iron nanoparticles synthesized by a tea extract. Journal of Cleaner Production. 2020;242:118476.
59. Ali RM, Hamad HA, Hussein MM, Malash GF. Potential of using green adsorbent of heavy metal removal from aqueous solutions: Adsorption kinetics, isotherm, thermodynamic, mechanism and economic analysis. Ecological Engineering. 2016;91:317-32.
60. Kumar S, Nair RR, Pillai PB, Gupta SN, Iyengar MAR, Sood AK. Graphene Oxide–MnFe2O4 Magnetic Nanohybrids for Efficient Removal of Lead and Arsenic from Water. ACS Applied Materials & Interfaces. 2014;6(20):17426-36.